

Electronic Structure and Enhanced Charge-Density Wave Order of Monolayer VSe_2

Jiagui Feng,^{†,‡,||} Deepnarayan Biswas,^{†,||} Akhil Rajan,^{†,||} Matthew D. Watson,[†] Federico Mazzola,[†] Oliver J. Clark,[†] Kaycee Underwood,[†] Igor Marković,^{†,§} Martin McLaren,[†] Andrew Hunter,[†] David M. Burn,^{||} Liam B. Duffy,^{⊥,#} Sourabh Barua,^{∇,★} Geetha Balakrishnan,[∇] François Bertran,[○] Patrick Le Fèvre,[○] Timur K. Kim,[◆] Gerrit van der Laan,^{||} Thorsten Hesjedal,^{⊥,Ⓛ} Peter Wahl,^{†,Ⓛ} and Phil D. C. King^{*,†,Ⓛ}

[†]SUPA, School of Physics and Astronomy, University of St. Andrews, St. Andrews KY16 9SS, United Kingdom

[‡]Suzhou Institute of Nano-Technology and Nanobionics (SINANO), CAS, 398 Ruoshui Road, SEID, SIP, Suzhou 215123, China

[§]Max Planck Institute for Chemical Physics of Solids, Nöthnitzer Straße 40, 01187 Dresden, Germany

^{||}Magnetic Spectroscopy Group, Diamond Light Source, Didcot OX11 0DE, United Kingdom

[⊥]Department of Physics, University of Oxford, Oxford OX1 3PU, United Kingdom

[#]ISIS, STFC, Rutherford Appleton Laboratory, Didcot OX11 0QX, United Kingdom

[∇]Department of Physics, University of Warwick, Coventry CV4 7AL, United Kingdom

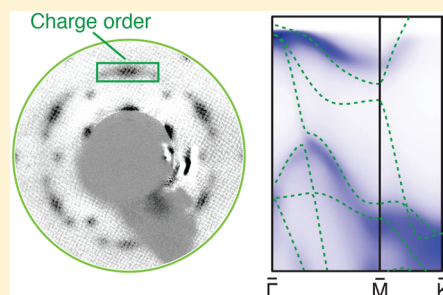
[○]Synchrotron SOLEIL, CNRS-CEA, L'Orme des Merisiers, Saint-Aubin-BP48, 91192 Gif-sur-Yvette, France

[◆]Diamond Light Source, Harwell Campus, Didcot OX11 0DE, United Kingdom

Supporting Information

ABSTRACT: How the interacting electronic states and phases of layered transition-metal dichalcogenides evolve when thinned to the single-layer limit is a key open question in the study of two-dimensional materials. Here, we use angle-resolved photoemission to investigate the electronic structure of monolayer VSe_2 grown on bilayer graphene/SiC. While the global electronic structure is similar to that of bulk VSe_2 , we show that, for the monolayer, pronounced energy gaps develop over the entire Fermi surface with decreasing temperature below $T_c = 140 \pm 5$ K, concomitant with the emergence of charge-order superstructures evident in low-energy electron diffraction. These observations point to a charge-density wave instability in the monolayer that is strongly enhanced over that of the bulk. Moreover, our measurements of both the electronic structure and of X-ray magnetic circular dichroism reveal no signatures of a ferromagnetic ordering, in contrast to the results of a recent experimental study as well as expectations from density functional theory. Our study thus points to a delicate balance that can be realized between competing interacting states and phases in monolayer transition-metal dichalcogenides.

KEYWORDS: VSe_2 , charge-density wave, transition-metal dichalcogenide, monolayer



Control over material thickness down to the single-atom scale has emerged as a powerful tuning parameter for manipulating not only the single-particle band structures of solids but also, and increasingly, their interacting electronic states and phases.^{1–7} A particularly attractive materials system in which to explore this is the transition-metal dichalcogenides (TMDs), both because of their naturally layered van der Waals structures and because of the wide variety of materials properties that they are known to host.^{4–13} These include much-studied charge-density wave (CDW) states^{14–18} that exhibit an intricate interplay with superconductivity in several TMDs.^{19–22} Yet, a consistent picture is still to emerge over how their charge-ordered states evolve when reducing materials thickness down to a single monolayer.^{23–29}

In part, this reflects an intrinsic competition, whereby the microscopic interactions that drive such phase formation and the fluctuations that destabilize it are both expected to become strengthened in the two-dimensional limit compared to their bulk three-dimensional counterparts. Here, we investigate VSe_2 as a particularly attractive candidate system in which to probe such phenomenology. It is known to host a CDW in the bulk with an onset temperature of $T_c \approx 110$ K.^{15,30} Despite its simple layered structure (Figure 1a), the $(4 \times 4 \times 3)$ CDW reconstruction of the bulk has a significant component in the out-of-plane direction,^{15,30} which has been attributed to a

Received: April 24, 2018

Revised: May 30, 2018

Published: June 18, 2018

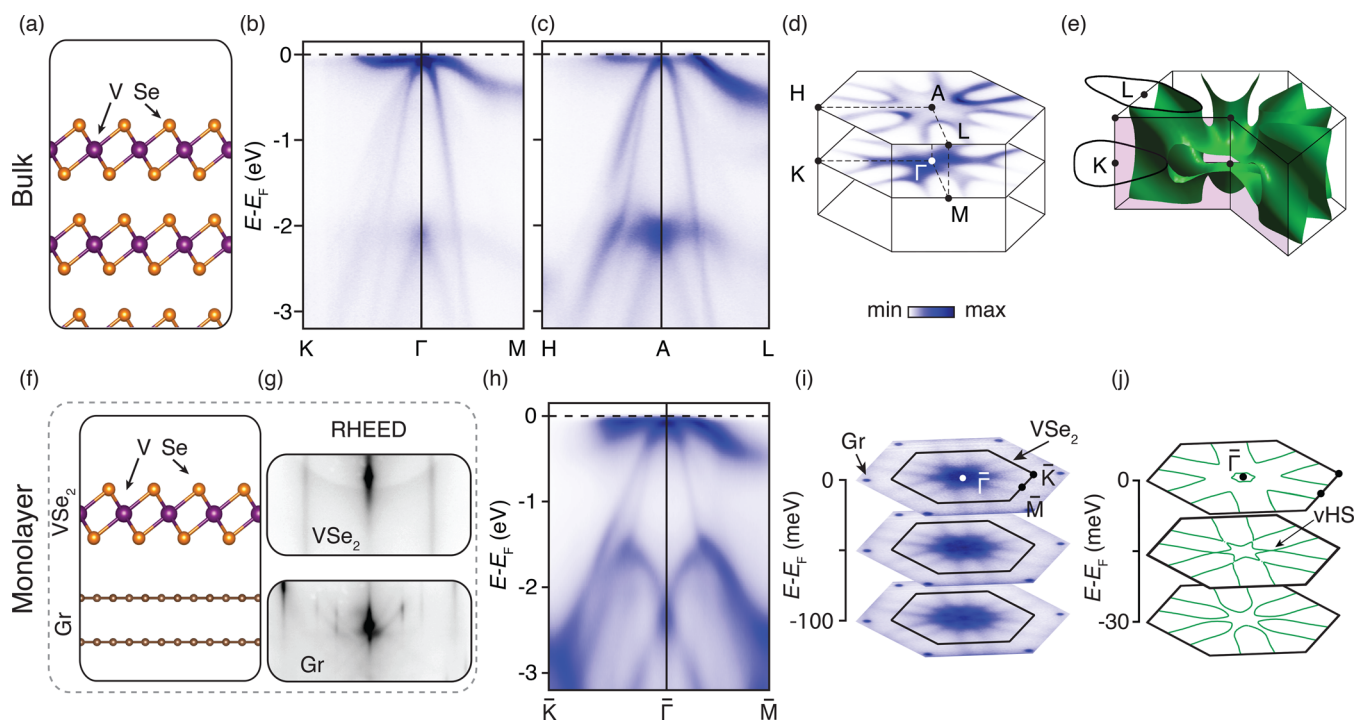


Figure 1. Normal-state electronic structure of bulk and monolayer VSe_2 . (a) $1T$ crystal structure of bulk VSe_2 and (b,c) its normal-state electronic structure ($T \approx 170$ K) measured along the (b) $\text{K}-\Gamma-\text{M}$ ($k_z \approx 0$, $h\nu = 92.5$ eV) and (c) $\text{H}-\text{A}-\text{L}$ ($k_z \approx \pi/c$, $h\nu = 110$ eV) directions of the bulk Brillouin zone. (d) Corresponding Fermi surfaces measured in the $\text{K}-\Gamma-\text{M}$ and $\text{H}-\text{A}-\text{L}$ planes and (e) calculated DFT Fermi surface throughout the three-dimensional Brillouin zone. (f) Crystal structure of VSe_2 /bilayer graphene (Gr) heterostructure and (g) RHEED measured along the $[\bar{1}\bar{1}00]$ direction of the graphene substrate (bottom) and following the growth of ML VSe_2 (top). (h) Electronic structure ($T = 170$ K) of monolayer VSe_2 measured along the $\bar{\text{K}}-\bar{\Gamma}-\bar{\text{M}}$ direction ($h\nu = 21.2$ eV). (i, j) Corresponding (i) measured ($h\nu = 110$ eV) and (j) calculated Fermi surface and near- E_F constant energy contours of monolayer VSe_2 , revealing the close proximity of the van Hove singularity to the Fermi level.

nesting of the strongly three-dimensional Fermi surface at the corresponding wave vector.³¹ Reducing the material thickness to a single monolayer (ML), where the electronic structure must become strictly two-dimensional, could therefore be expected to have a major influence on the charge order in VSe_2 . Studies of multilayer exfoliated flakes have so far indicated both a strengthening and a suppression of its CDW with reducing thickness,^{23,32,33} necessitating further studies in the true monolayer limit.

Moreover, first-principles calculations have consistently predicted that a robust ferromagnetic order should emerge for monolayer VSe_2 , with a pronounced exchange splitting of the near- E_F electronic states in the $1T$ polymorph of more than 500 meV.^{32,34} A very recent experimental report that such a ferromagnetic state persists up to room temperature in monolayer VSe_2 ³⁵ raised the tantalizing prospect that this system could form one of the emerging class of 2D magnets.^{36,37} There are, however, a number of critical unexplained features such as a reported magnetization as high as $15 \mu_B$ per vanadium atom, motivating further investigation of this putative ferromagnetic state.

In this work, we synthesize monolayer VSe_2 films on both bilayer graphene/SiC and highly oriented pyrolytic graphite (HOPG) substrates using molecular-beam epitaxy (see the Methods section). We use both in situ and synchrotron-based angle-resolved photoemission spectroscopy (ARPES) to directly probe their temperature-dependent electronic structure and search for ferromagnetic order from X-ray magnetic circular dichroism (XMCD). Our measurements indicate no ferromagnetism down to 10 K. Instead, they reveal that a

charge-density wave that gaps the entire high-temperature Fermi surface is the dominant instability at low temperatures in monolayer VSe_2 .

Figure 1 summarizes the normal-state electronic structure of bulk and monolayer VSe_2 from our ARPES measurements of single-crystal samples and epitaxial monolayers, respectively. Both the bulk and the monolayer samples host a qualitatively similar electronic structure. The Fermi surface is formed from a relatively weakly dispersive V $3d$ -electron-derived band.³⁸ An additional set of hole-like bands, derived from the Se $4p$ orbitals, disperse steeply down from the Γ point into the lower-lying valence bands, with their band maximum situated 65 meV below E_F .

In bulk, the Fermi surface of VSe_2 is known to be three-dimensional.³¹ Consistent with this, we find subtle but important differences in the electronic structure measured using photon energies chosen to probe close to the center and boundary of the Brillouin zone along k_z , respectively (Figure 1b–d). In particular, the V-derived state crosses E_F along the A–L direction, leading to a Fermi surface which forms closed electron-like contours of almost elliptical cross-section enclosing the zone-edge L-points in the H–A–L plane. In contrast, this band does not quite reach E_F along the Γ –M direction, with the clear Fermi crossing along Γ –K instead forming the tip of a large trigonally warped hole-like Fermi contour located around each corner K-point within the $\text{K}-\Gamma-\text{M}$ plane. This is in agreement with the calculated Fermi surface from density functional theory (DFT, Figure 1e) as well as previous soft X-ray ARPES measurements,³¹ which

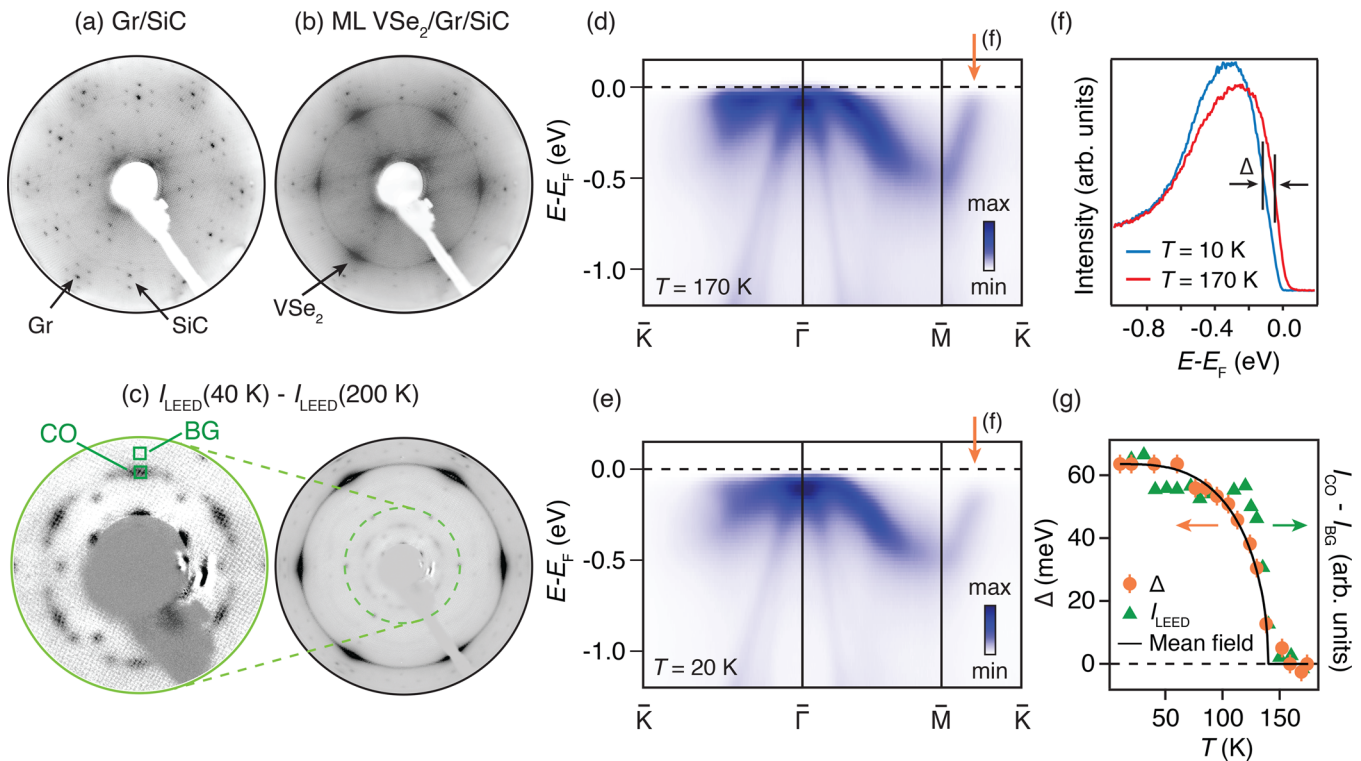


Figure 2. Charge-density wave order of monolayer VSe_2 . (a, b) Low-energy electron diffraction of (a) bilayer Graphene/SiC and (b) following additional growth of ML- VSe_2 ($T = 170$ K, $E = 150$ eV). (c) Differences of ML- VSe_2 LEED ($E = 100$ eV) at $T = 40$ and 200 K, revealing the emergence of additional charge-order peaks at low temperatures, as shown as magnified and with enhanced contrast in the inset. (d, e) Corresponding evolution of the measured electronic structure ($h\nu = 21.2$ eV) from (d) $T = 170$ K to (e) $T = 20$ K, revealing the opening of a charge-density wave gap at the Fermi level. (f) This is clearly evident in EDCs at k_F along the $\bar{M}-\bar{K}$ direction (at the position marked in panels d and e). (g) The temperature-dependent shift of the leading edge midpoint (LEM) of these EDCs, Δ (left), is in good agreement with the intensity-dependence of the charge-order superstructure from LEED, plotted as $I_{\text{CO}} - I_{\text{BG}}$ to take account of temperature-dependent background variations, in which the charge order and background regions are defined in panel c. The solid line in panel g shows a fit to a semiphenomenological mean-field form for the gap opening, $\Delta(T) \propto \tanh\left(C\sqrt{\frac{T_c}{T} - 1}\right)$, where C is a constant.

indicate the k_z -dependent evolution of the Fermi surface between these two distinct topologies.

In contrast, the Fermi surface of ML- VSe_2 must be strictly two-dimensional. Our measured Fermi surface (Figure 1i) exhibits nearly triangular hole-like pockets around the corner \bar{K} -points of the 2D Brillouin zone. This is most similar to the bulk Fermi surface for the $k_z = 0$ plane. Moving below the Fermi level, the constant energy contours evolve into closed electron-like pockets centered around the \bar{M} -points, similar to the bulk Fermi surface within the $k_z = \pi/c$ plane. Our DFT calculations (Figure 1j) indicate that the van Hove singularity that marks the transition between these cases is situated within ~ 20 meV of the Fermi level. From our measured dispersions along $\bar{\Gamma}-\bar{K}$, we find experimentally that this van Hove singularity is located at a slightly higher binding energy of 45 meV. This may reflect a slight electron doping of our monolayer films due to charge transfer from the substrate. Nonetheless, its proximity to the Fermi level raises the tantalizing prospect of driving a Lifshitz transition in monolayer VSe_2 by moderate charge-carrier doping via either chemical substitution or transistor-style gating approaches.

The π -states of the underlying bilayer graphene substrate are also visible in our measurements, situated on the vertices of a hexagon in Figure 1i, where they are evident as small electron pockets due to the residual electron doping of our epitaxial graphene samples. The Brillouin zone of the VSe_2 lattice is in good rotational alignment with the graphene one but is

smaller. This points to a weak coupling between the substrate and the overlayer, such that strain is not coupled into the as-grown film. This is consistent with our reflection high-energy electron diffraction (RHEED, Figure 1g) measurements, which indicate an in-plane lattice constant of our monolayer VSe_2 of $a = 3.31 \pm 0.05$ Å, in good agreement with that of bulk VSe_2 . This is further supported by our low-energy electron diffraction (LEED) measurements (Figure 2a–c). Sharp Bragg spots and a well-defined Moiré superstructure, arising due to the lattice mismatch between graphene and SiC, are observed for our bilayer graphene/SiC substrates (Figure 2a). As is typical for epitaxial TMD monolayers,^{28,39,40} the Bragg spots of our VSe_2 are rather elongated in the azimuthal direction (Figure 2b), indicating some rotational disorder due to the weak substrate–overlayer interaction. Their intensity is, however, strongly peaked in the direction parallel to the Bragg spots of the graphene lattice, indicating that they retain a good overall epitaxial registry.

At low temperatures, a new set of features appear in our LEED measurements (Figure 2c), labeled “CO” in the magnified image. These show a similar angular spread as for the VSe_2 Bragg spots discussed above but are much weaker in overall intensity. We assign these as charge-order peaks indicative of a CDW instability persisting to the monolayer limit of VSe_2 , as further supported below. The location of the new features that we observe in LEED is consistent with the $\bar{\Gamma}\{11\}$ family of charge order spots for a (4×4) CDW order,

retaining the in-plane periodicity of the bulk CDW,^{15,30,41} where the $\bar{\Gamma}\{01\}$ spots would be shadowed by the electron gun in our LEED optics. Although this is certainly plausible, further measurements, for example scanning tunnelling microscopy or X-ray scattering, will be required to unambiguously classify \mathbf{q}_{CDW} here. Irrespective of the precise ordering vector, we show below how this CDW has a pronounced effect on the low-energy electronic structure of monolayer VSe_2 .

At the Fermi crossing along the $\bar{M}-\bar{K}$ direction, a pronounced CDW gap opens, evident as a shift of $\Delta = 64 \pm 5$ meV of the leading edge midpoint (LEM) of EDCs measured at the k_{F} of the normal-state Fermi surface (Figure 2f). Monitoring this leading-edge shift as a function of temperature (Figure 2g), we observe a gap opening that closely follows the intensity of the charge-order superstructure peak that we observe in LEED. These both onset at $T_c = 140 \pm 5$ K, providing unambiguous evidence that charge-density wave order not only persists to but also is strengthened in the monolayer limit of VSe_2 . This is consistent with transport studies of few-layer VSe_2 obtained by liquid exfoliation³² as well as the very recent observation of an increasing T_c with decreasing material thickness extracted from scanning tunnelling microscopy measurements of mechanically exfoliated few-layer samples.³³

The CDW gap opening is reasonably described by a semi-phenomenological mean-field functional form (Figure 2g). For a two-dimensional system such as this, fluctuations would be expected to reduce the temperature at which long-range order sets in. Given the relatively large line widths of our measured EDCs (see the Methods section), we cannot conclusively say whether these lead to deviations from a mean-field form for the gap opening in close vicinity to T_c . Irrespective, the clear spectroscopic gap opening that we observe here at 140 ± 5 K points to a robust enhancement of the T_c for monolayer VSe_2 , as compared to the bulk T_c of 110 K.

Our measured low-temperature gap magnitude and CDW transition temperature yield a value of $2\Delta/k_{\text{B}}T_c \approx 10$, which significantly exceeds the value of 3.52 that would be expected for a weak-coupling mean-field instability. In agreement with this, Figure 3a,b shows how the closed Fermi pockets around the \bar{K} -points that are evident at high temperatures lose almost all of their spectral weight below T_c . This indicates that the entire Fermi surface becomes gapped by the CDW, rather than only its well-nested portions. Indeed, EDCs taken at the apex of the Fermi surface along $\bar{\Gamma}-\bar{K}$ (Figure 3c) indicate a similar temperature-dependent gap opening (Figure 3d) to that discussed above for the Fermi crossing along $\bar{M}-\bar{K}$, albeit with a smaller gap magnitude of $\Delta = 30 \pm 5$ meV.

This is in stark contrast to bulk VSe_2 , where gaps are thought to only open over small portions of the Fermi surface that are well-nested.³¹ In the monolayer, we find that the flat portions of Fermi surface have a nesting vector along \mathbf{a}^* of $\mathbf{q}_{\text{nest}} = 0.54 \pm 0.04 \text{ \AA}^{-1}$, which is close to the ordering wavevector of the CDW discussed above. Nonetheless, while this may help to enhance the CDW order, the large overall gap magnitude (particularly persisting to the tips of the Fermi surface, where there is negligible nesting) instead points to a strong electron-phonon coupling as the main driver of the CDW instability here. Similarly, we note that the apparently even better Fermi surface nesting along the one-dimensional directions at 30° rotation from the \mathbf{a}^* direction that is evident in Figure 1i,j does not appear to dominate the CDW ordering vector here, further confirming that nesting is not the driving force of the CDW in

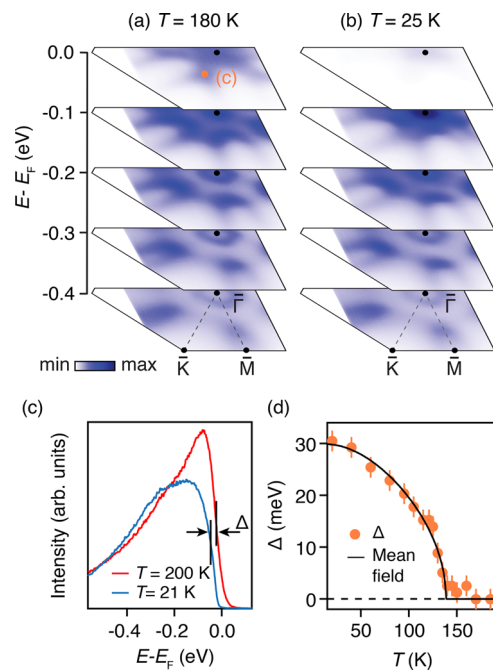


Figure 3. Momentum-dependent CDW gaps. Fermi surface of monolayer VSe_2 measured ($h\nu = 21.2$ eV) at (a) $T = 180$ K and (b) $T = 20$ K. (c) Corresponding EDCs at the tip of the \bar{K} -centered Fermi surface (orange dot in panel a) and (d) temperature-dependent gap opening extracted from the LEM shift of such EDCs, together with a mean-field fit (solid line).

monolayer VSe_2 . Consistent with this, we also find a fully- or near-fully gapped CDW phase from our measurements on HOPG substrates (Supplementary Figure S1), with a critical temperature ($T_c = 134 \pm 5$ K) comparable to the measurements shown here for graphene substrates.

Finally, we return to the question of whether monolayer VSe_2 hosts an intrinsic ferromagnetic state. Indeed, consistent with previous calculations,^{32,34} our DFT of single-layer VSe_2 indicates that a ferromagnetic ground state is the lowest energy configuration. Comparing the calculated electronic structure in the ferromagnetic state (Figure 4a) with equivalent non-magnetic calculations (Figure 4b), the ferromagnetism can be seen to dominantly affect the V-derived states, inducing a splitting of ~ 500 meV between the spin majority and minority bands near the Fermi level. Such a pronounced exchange splitting is inconsistent with our experimental measurements (Figure 4c), where only a single d -band dispersion is observed. Indeed, the overall band dispersions observed experimentally are entirely consistent with the nonmagnetic calculation apart from a small difference in doping and an over-estimation of the bandwidth of the near- E_{F} states by a factor of ~ 1.4 , likely arising due to moderate electronic correlations associated with the V $3d$ orbitals that are not captured in DFT.

A lack of ferromagnetism here is further supported by measurements of V $L_{2,3}$ -edge X-ray magnetic circular dichroism (XMCD) from our monolayer VSe_2 samples, shown in Figure 4d. XMCD is a sensitive element-specific probe of magnetic order. Despite this, we find negligible dichroism either when measured in an applied magnetic field of 9 T or when measured in remanence and at temperatures of 300 or 100 K (Figure 4d). This directly rules out any ferromagnetic order of monolayer VSe_2 down to $T = 100$ K, in stark contrast to the recent report of robust ferromagnetism at room temperature in

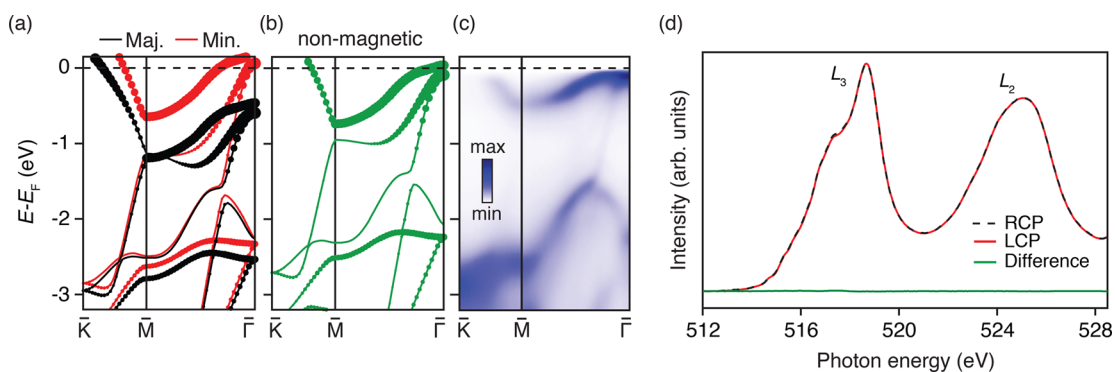


Figure 4. Absence of ferromagnetic order. Electronic structure of monolayer VSe_2 from (a) a spin-polarized and (b) a nonmagnetic DFT calculation. The calculations are projected onto the V $3d$ orbital character (size of the points), and the majority and minority spin components are shown, respectively, as black and red coloring in panel a. (c) Equivalent experimental electronic structure, which is consistent only with the nonmagnetic calculation. (d) V $L_{2,3}$ -edge X-ray absorption measurements performed using left-circularly polarized (LCP) and right-circularly polarized (RCP) light in an applied magnetic field of 9 T ($T = 100$ K, red and black lines, respectively) and corresponding difference signal (green) show the absence of XMCD, further ruling out ferromagnetic order.

this system.³⁵ The absence of an exchange splitting in the electronic structure, discussed above, further allows us to exclude that ferromagnetism develops down to our lowest ARPES measurement temperature of $T = 10$ K.

It remains an open question as to why our DFT calculations, consistent with previous literature,^{32,34} dramatically overestimate the tendency for ferromagnetism in monolayer VSe_2 . We speculate that phase fluctuations in the two-dimensional limit may play a more important role for the ferromagnetic state here, renormalizing its energy scale to below that at which the CDW takes over as the dominant instability. The consequent full gapping of the Fermi surface that we observe would then remove the driving force for a Stoner-type ferromagnetic order.⁴² This suggests an appealing potential for engineering competition between disparate ground states in ML- VSe_2 and other TMDs. These may be tunable by, for example, charge-carrier doping or promoting magnetic order via proximity effects. Beyond this, our study demonstrates how charge order can be readily manipulated in two-dimensional materials, here not only occurring with a significantly increased T_c as compared to the bulk but also exhibiting signatures of a much stronger-coupling instability in the single-layer limit of VSe_2 .

Methods. Molecular-Beam Epitaxy. Our films are grown using molecular-beam epitaxy on epitaxial bilayer graphene/ SiC as well as highly oriented pyrolytic graphite (HOPG) substrates in a UHV chamber with a base pressure of $\sim 1 \times 10^{-10}$ mbar. A high-temperature effusion cell with 4N pure V and a valved cracker cell with 5N pure Se are used as sources.

For a typical growth, the substrate is first annealed to 550°C for 60 min before cooling to a growth temperature of 300°C (thermocouple temperature). During growth, the V flux is maintained at a beam-equivalent pressure (BEP) of $\sim 6 \times 10^{-10}$ mbar, whereas approximately an order of magnitude greater Se flux is used. Our growth rate of 1 ML per hour is dictated by the V flux due to the near unity sticking coefficient of V at the growth temperature. As growth progresses, the streaky RHEED patterns visible from both graphene and HOPG substrates gradually disappear and the new VSe_2 streaks begin to appear (see Figure S2). These new patterns become strong and streaky toward the end of the growth, confirming the flat morphology of the monolayer VSe_2 surface. This, as well as a nearly uniform ML surface coverage, are confirmed by atomic

force microscopy (Figure S3). Some samples were capped with a protective Se layer after growth. For these, the samples are cooled down to below 35°C before depositing an amorphous layer of Se for 10 min. The Se BEP is maintained at $\sim 8 \times 10^{-7}$ mbar, which provides an estimated deposition rate of 1 nm/min.

For substrates, fresh HOPG surfaces were exfoliated in atmosphere and straight-away transferred into a vacuum load lock. For graphene synthesis, we used a variation of a widely demonstrated technique for epitaxial bilayer graphene growth:⁴³ 3×7 mm² wafers of n -type 6H- SiC (0001) were first cleaned using acetone and isopropanol. A pair of such substrates were then placed one on top of another with the Si terminated surfaces facing each other and a 0.12 mm thick Ta spacer between them on both ends. This “sandwich” was then loaded into a vacuum chamber and annealed at 600°C for 6 h by direct current heating. After this, the substrates were further heated to 1500°C for 7 min to produce bilayer graphene layers. These yield sharp Bragg spots and well-defined Moiré patterns in LEED measurements (Figure 2a).

Angle-Resolved Photoemission. Following growth, our samples were transferred in situ to a lab-based ARPES setup. ARPES measurements were performed using a high-intensity He lamp ($h\nu = 21.2$ eV, p polarization) and a SPECS Phoibos 225 hemispherical electron analyzer at temperatures between 10 and 180 K. LEED measurements were performed in the same system using a SPECS ErLEED 150. We note that the measured line widths of our EDCs are significantly higher than the experimental energy resolution, in common with other ARPES studies of monolayer TMDs. This could reflect impurity scattering, finite domain-size effects, and the effects of rotational disorder. The resultant broadening can lead to an under-estimation of the CDW gap size from the LEM shift, although we stress that this analysis method still yields a robust value of T_c .

Monolayer VSe_2 samples were also measured at the I05 beamline of Diamond Light Source using photon energies of 92.5 and 110 eV and a Scienta R4000 analyzer. The measurements shown in Figure 1i are the sum of Fermi surfaces recorded using left- and right-circularly polarized light. The samples were Se-capped following growth, as described above, and transferred through air before being decapped by annealing to $\sim 230^\circ\text{C}$ for 15 min in a preparation chamber

connected to the I05 ARPES chamber. Characterization by LEED and ARPES in our home system indicates that the capping, air exposure, and decapping procedure leads to no noticeable changes in the measured electronic structure. In addition, ARPES measurements of bulk VSe₂ crystals⁴⁴ were performed using the I05 beamline as well as the CASSIOPEE beamline of the SOLEIL synchrotron, France, using Scienta R4000 electron analyzers. The data shown in Figure 1b,c is the sum of measurements performed using *p*- and *s*-polarized light, while *p*-polarized light is used for the Fermi surfaces shown in Figure 1d. The samples were cleaved in situ and measured at a temperature of 170 K.

Calculations. The electronic structure of monolayer VSe₂ was calculated within density functional theory. The DFT calculations were performed using the Wien2k package,⁴⁵ utilizing the linearized augmented plane wave (LAPW) method and the Perdew Burke and Ernzerhof (PBE) exchange-correlation functional.⁴⁶ A separation of 18 Å between V layers in our supercell (corresponding to a vacuum gap of 14.85 Å) was found to be sufficient to ensure our calculations were representative of an isolated monolayer. We employed a 14 × 14 × 2 k-point mesh, and the internal lattice parameters were optimized until the total force is less than 2 mRy/a.u.

X-ray Magnetic Circular Dichroism. XMCD measurements were performed in total electron yield (TEY) mode from Se-capped samples at the ID32 beamline of the ESRF synchrotron. The sample was mounted with the incoming X-ray beam at 55° to the surface normal. The V L_{2,3}-edge X-ray absorption was clearly visible in TEY mode but was only very weakly evident when measuring in fluorescence mode due to the monolayer thickness. XMCD measurements were performed first at room temperature in an applied magnetic field of 9 T and then in remanence. This measurement cycle was repeated after cooling to 100 K. All measurements yielded a consistent result of negligible dichroism.

■ ASSOCIATED CONTENT

Supporting Information

The Supporting Information is available free of charge on the ACS Publications website at DOI: 10.1021/acs.nanolett.8b01649.

Figures showing equivalent measurements to those shown in the main text for samples grown on HOPG substrates and additional growth and materials characterization from reflection high-energy electron diffraction and atomic force microscopy. (PDF)

■ AUTHOR INFORMATION

Corresponding Author

*E-mail: philip.king@st-andrews.ac.uk.

ORCID

Thorsten Hesjedal: 0000-0001-7947-3692

Peter Wahl: 0000-0002-8635-1519

Phil D. C. King: 0000-0002-6523-9034

Present Address

*Department of Physics, Birla Institute of Technology, Mesra 835215, Ranchi, India

Author Contributions

[†]J.F., D.B., and A.R. contributed equally.

Notes

The authors declare no competing financial interest.

■ ACKNOWLEDGMENTS

We thank Andrew Huxley for useful discussions. We gratefully acknowledge support from The Leverhulme Trust (grant nos. RL-2016-006 and PLP-2015-144); The Royal Society; The Engineering and Physical Sciences Research Council, U.K., for support under grant nos. EP/I031014/1, EP/M023958/1, EP/P020151/1, EP/M028771/1, and EP/L014963/1; and the International Max-Planck Partnership for Measurement and Observation at the Quantum Limit. O.J.C. and K.U. acknowledge EPSRC for PhD studentship support through grant nos. EP/K503162/1 and EP/L015110/1. I.M. acknowledges PhD studentship support from the IMPRS for the Chemistry and Physics of Quantum Materials. L.B.D. acknowledges studentship support from EPSRC and the Science and Technology Facilities Council (U.K.). We thank Diamond Light Source for access to beamline I05 (proposal no. SI19771-1), SOLEIL for access to the CASSIOPEE beamline, and the ESRF for access to the ID32 beamline, all of which contributed to the results presented here. Finally, we are grateful to Andreas Frisk for assistance with the XMCD measurements. The research data supporting this publication can be accessed at <http://dx.doi.org/10.17630/2dbe6c40-e68a-46f6-8903-9bdf6731433c>.

■ REFERENCES

- (1) Mak, K. F.; Lee, C.; Hone, J.; Shan, J.; Heinz, T. F. Atomically Thin MoS₂: A New Direct-Gap Semiconductor. *Phys. Rev. Lett.* **2010**, *105*, 136805.
- (2) Mannhart, J.; Schlom, D. G. Oxide Interfaces – an Opportunity for Electronics. *Science* **2010**, *327*, 1607–1611.
- (3) Hwang, H. Y.; Iwasa, Y.; Kawasaki, M.; Keimer, B.; Nagaosa, N.; Tokura, Y. Emergent Phenomena at Oxide Interfaces. *Nat. Mater.* **2012**, *11*, 103–113.
- (4) Wang, Q. H.; Kalantar-Zadeh, K.; Kis, A.; Coleman, J. N.; Strano, M. S. Electronics and Optoelectronics of Two-dimensional Transition Metal Dichalcogenides. *Nat. Nanotechnol.* **2012**, *7*, 699–712.
- (5) Geim, A. K.; Grigorieva, I. V. Van der Waals Heterostructures. *Nature* **2013**, *499*, 419–425.
- (6) Xu, X.; Yao, W.; Xiao, D.; Heinz, T. F. Spin and Pseudospins in Layered Transition Metal Dichalcogenides. *Nat. Phys.* **2014**, *10*, 343–350.
- (7) Ajayan, P.; Kim, P.; Banerjee, K. Two-dimensional Van Der Waals Materials. *Phys. Today* **2016**, *69*, 38–44.
- (8) Chhowalla, M.; Shin, H. S.; Eda, G.; Li, L.-J.; Loh, K. P.; Zhang, H. The Chemistry of Two-dimensional Layered Transition Metal Dichalcogenide Nanosheets. *Nat. Chem.* **2013**, *5*, 263–275.
- (9) Riley, J. M.; Mazzola, F.; Dendzik, M.; Michiardi, M.; Takayama, T.; Bawden, L.; Granerød, C.; Leandersson, M.; Balasubramanian, T.; Hoesch, M.; Kim, T. K.; Takagi, H.; Meevasana, W.; Hofmann, P.; Bahramy, M. S.; Wells, J. W.; King, P. D. C. Direct Observation of Spin-polarized Bulk Bands in an Inversion-symmetric Semiconductor. *Nat. Phys.* **2014**, *10*, 835–839.
- (10) Lu, J. M.; Zheliuk, O.; Leermakers, I.; Yuan, N. F. Q.; Zeitler, U.; Law, K. T.; Ye, J. T. Evidence for Two-dimensional Ising Superconductivity in Gated MoS₂. *Science* **2015**, *350*, 1353–1357.
- (11) Riley, J. M.; Meevasana, W.; Bawden, L.; Asakawa, M.; Takayama, T.; Eknepakul, T.; Kim, T. K.; Hoesch, M.; Mo, S.-K.; Takagi, H.; Sasagawa, T.; Bahramy, M. S.; King, P. D. C. Negative Electronic Compressibility and Tunable Spin Splitting in WSe₂. *Nat. Nanotechnol.* **2015**, *10*, 1043–1047.
- (12) Kogar, A.; Rak, M. S.; Vig, S.; Husain, A. A.; Flicker, F.; Joe, Y. I.; Venema, L.; MacDougall, G. J.; Chiang, T. C.; Fradkin, E.; van

Wezel, J.; Abbamonte, P. Signatures of Exciton Condensation in a Transition Metal Dichalcogenide. *Science* **2017**, *358*, 1314–1317.

(13) Bahramy, M. S.; Clark, O. J.; Yang, B.-J.; Feng, J.; Bawden, L.; Riley, J. M.; Marković, I.; Mazzola, F.; Sunko, V.; Biswas, D.; Cooil, S. P.; Jorge, M.; Wells, J. W.; Leandersson, M.; Balasubramanian, T.; Fujii, J.; Vobornik, I.; Rault, J. E.; Kim, T. K.; Hoesch, M.; Okawa, K.; Asakawa, M.; Sasagawa, T.; Eknapakul, T.; Meevasana, W.; King, P. D. C. Ubiquitous Formation of Bulk Dirac Cones and Topological Surface States from a Single Orbital Manifold in Transition-metal Dichalcogenides. *Nat. Mater.* **2017**, *17*, 21.

(14) Wilson, J. A.; Di Salvo, F. J.; Mahajan, S. Charge-Density Waves in Metallic, Layered, Transition-Metal Dichalcogenides. *Phys. Rev. Lett.* **1974**, *32*, 882–885.

(15) Tsutsumi, K. X-ray-diffraction Study of the Periodic Lattice Distortion Associated with a Charge-density Wave in 1T-VSe₂. *Phys. Rev. B: Condens. Matter Mater. Phys.* **1982**, *26*, 5756–5759.

(16) Johannes, M. D.; Mazin, I. I.; Howells, C. A. Fermi-surface Nesting and the Origin of the Charge-density Wave in NbSe₂. *Phys. Rev. B: Condens. Matter Mater. Phys.* **2006**, *73*, 205102.

(17) Borisenko, S. V.; Kordyuk, A. A.; Yaresko, A. N.; Zabolotnyy, V. B.; Inosov, D. S.; Schuster, R.; Büchner, B.; Weber, R.; Follath, R.; Patthey, L.; Berger, H. Pseudogap and Charge Density Waves in Two Dimensions. *Phys. Rev. Lett.* **2008**, *100*, 196402.

(18) Bawden, L.; Cooil, S. P.; Mazzola, F.; Riley, J. M.; Collins-McIntyre, L. J.; Sunko, V.; Hunvik, K. W. B.; Leandersson, M.; Polley, C. M.; Balasubramanian, T.; Kim, T. K.; Hoesch, M.; Wells, J. W.; Balakrishnan, G.; Bahramy, M. S.; King, P. D. C. Spin-valley Locking in the Normal State of a Transition-metal Dichalcogenide Superconductor. *Nat. Commun.* **2016**, *7*, 11711.

(19) Morosan, E.; Zandbergen, H. W.; Dennis, B. S.; Bos, J. W. G.; Onose, Y.; Klimczuk, T.; Ramirez, A. P.; Ong, N. P.; Cava, R. J. Superconductivity in Cu_xTiSe₂. *Nat. Phys.* **2006**, *2*, 544–550.

(20) Kiss, T.; Yokoya, T.; Chainani, A.; Shin, S.; Hanaguri, T.; Nohara, M.; Takagi, H. Charge-order-maximized Momentum-dependent Superconductivity. *Nat. Phys.* **2007**, *3*, 720–725.

(21) Rahn, D. J.; Hellmann, S.; Kalläne, M.; Sohr, C.; Kim, T. K.; Kipp, L.; Rossnagel, K. Gaps and Kinks in the Electronic Structure of the Superconductor 2H-NbSe₂ from Angle-resolved Photoemission at 1 K. *Phys. Rev. B: Condens. Matter Mater. Phys.* **2012**, *85*, 224532.

(22) Li, L. J.; O'Farrell, E. C. T.; Loh, K. P.; Eda, G.; Özyilmaz, B.; Castro Neto, A. H. Controlling Many-body States by the Electric-field Effect in a Two-dimensional Material. *Nature* **2016**, *529*, 185–189.

(23) Yang, J.; Wang, W.; Liu, Y.; Du, H.; Ning, W.; Zheng, G.; Jin, C.; Han, Y.; Wang, N.; Yang, Z.; Tian, M.; Zhang, Y. Thickness Dependence of the Charge-density-wave Transition Temperature in VSe₂. *Appl. Phys. Lett.* **2014**, *105*, 063109.

(24) Xi, X.; Zhao, L.; Wang, Z.; Berger, H.; Forró, L.; Shan, J.; Mak, K. F. Strongly Enhanced Charge-density-wave Order in Monolayer NbSe₂. *Nat. Nanotechnol.* **2015**, *10*, 765–769.

(25) Yu, Y.; Yang, F.; Lu, X. F.; Yan, Y. J.; Cho, Y.-H.; Ma, L.; Niu, X.; Kim, S.; Son, Y.-W.; Feng, D.; Li, S.; Cheong, S.-W.; Chen, X. H.; Zhang, Y. Gate-tunable Phase Transitions in Thin Flakes of 1T-TaS₂. *Nat. Nanotechnol.* **2015**, *10*, 270–276.

(26) Yoshida, M.; Suzuki, R.; Zhang, Y.; Nakano, M.; Iwasa, Y. Memristive Phase Switching in Two-dimensional 1T-TaS₂ Crystals. *Sci. Adv.* **2015**, *1*, e1500606.

(27) Chen, P.; Chan, Y.-H.; Fang, X.-Y.; Zhang, Y.; Chou, M.-Y.; Mo, S.-K.; Hussain, Z.; Fedorov, A.-V.; Chiang, T.-C. Charge Density Wave Transition in Single-layer Titanium Diselenide. *Nat. Commun.* **2015**, *6*, 8943.

(28) Ugeda, M. M.; Bradley, A. J.; Zhang, Y.; Onishi, S.; Chen, Y.; Ruan, W.; Ojeda-Aristizabal, C.; Ryu, H.; Edmonds, M. T.; Tsai, H.-Z.; Riss, A.; Mo, S.-K.; Lee, D.; Zettl, A.; Hussain, Z.; Shen, Z.-X.; Crommie, M. F. Characterization of Collective Ground States in Single-layer NbSe₂. *Nat. Phys.* **2016**, *12*, 92–97.

(29) Ryu, H.; Chen, Y.; Kim, H.; Tsai, H.-Z.; Tang, S.; Jiang, J.; Liou, F.; Kahn, S.; Jia, C.; Omrani, A. A.; Shim, J. H.; Hussain, Z.; Shen, Z.-X.; Kim, K.; Min, B. I.; Hwang, C.; Crommie, M. F.; Mo, S.-

K. Persistent Charge-Density-Wave Order in Single-Layer TaSe₂. *Nano Lett.* **2018**, *18*, 689–694.

(30) Eaglesham, D. J.; Withers, R. L.; Bird, D. M. Charge-density-wave Transitions in 1T-VSe₂. *J. Phys. C: Solid State Phys.* **1986**, *19*, 359.

(31) Strocov, V. N.; Shi, M.; Kobayashi, M.; Monney, C.; Wang, X.; Krempasky, J.; Schmitt, T.; Patthey, L.; Berger, H.; Blaha, P. Three-Dimensional Electron Realm in VSe₂ by Soft-X-Ray Photoelectron Spectroscopy: Origin of Charge-Density Waves. *Phys. Rev. Lett.* **2012**, *109*, 086401.

(32) Xu, K.; Chen, P.; Li, X.; Wu, C.; Guo, Y.; Zhao, J.; Wu, X.; Xie, Y. Ultrathin Nanosheets of Vanadium Diselenide: A Metallic Two-Dimensional Material with Ferromagnetic Charge-Density-Wave Behavior. *Angew. Chem., Int. Ed.* **2013**, *52*, 10477–10481.

(33) Pásztor, Á.; Scarfato, A.; Barreateau, C.; Giannini, E.; Renner, C. Dimensional Crossover of the Charge Density Wave Transition in Thin Exfoliated VSe₂. *2D Mater.* **2017**, *4*, 041005.

(34) Ma, Y.; Dai, Y.; Guo, M.; Niu, C.; Zhu, Y.; Huang, B. Evidence of the Existence of Magnetism in Pristine VX₂ Monolayers (X = S, Se) and Their Strain-Induced Tunable Magnetic Properties. *ACS Nano* **2012**, *6*, 1695–1701.

(35) Bonilla, M.; Kolekar, S.; Ma, Y.; Diaz, H. C.; Kalappattil, V.; Das, R.; Eggers, T.; Gutierrez, H. R.; Phan, M.-H.; Batzill, M. Strong Room-temperature Ferromagnetism in VSe₂ Monolayers on Van der Waals Substrates. *Nat. Nanotechnol.* **2018**, *13*, 289–293.

(36) Gong, C.; Li, L.; Li, Z.; Ji, H.; Stern, A.; Xia, Y.; Cao, T.; Bao, W.; Wang, C.; Wang, Y.; Qiu, Z. Q.; Cava, R. J.; Louie, S. G.; Xia, J.; Zhang, X. Discovery of Intrinsic Ferromagnetism in Two-dimensional Van der Waals Crystals. *Nature* **2017**, *546*, 265–269.

(37) Huang, B.; Clark, G.; Navarro-Moratalla, E.; Klein, D. R.; Cheng, R.; Seyler, K. L.; Zhong, D.; Schmidgall, E.; McGuire, M. A.; Cobden, D. H.; Yao, W.; Xiao, D.; Jarillo-Herrero, P.; Xu, X. Layer-dependent Ferromagnetism in a Van der Waals Crystal down to the Monolayer Limit. *Nature* **2017**, *546*, 270–273.

(38) Zunger, A.; Freeman, A. J. Electronic Structure of 1T-VSe₂. *Phys. Rev. B: Condens. Matter Mater. Phys.* **1979**, *19*, 6001.

(39) Zhang, Y.; Chang, T.-R.; Zhou, B.; Cui, Y.-T.; Yan, H.; Liu, Z.; Schmitt, F.; Lee, J.; Moore, R.; Chen, Y.; Lin, H.; Jeng, H.-T.; Mo, S.-K.; Hussain, Z.; Bansil, A.; Shen, Z.-X. Direct Observation of the Transition from Indirect to Direct Bandgap in Atomically Thin Epitaxial MoSe₂. *Nat. Nanotechnol.* **2013**, *9*, 111–115.

(40) Jiao, L.; Liu, H. J.; Chen, J. L.; Yi, Y.; Chen, W. G.; Cai, Y.; Wang, J. N.; Dai, X. Q.; Wang, N.; Ho, W. K.; Xie, M. H. Molecular-beam Epitaxy of Monolayer MoSe₂: Growth Characteristics and Domain Boundary Formation. *New J. Phys.* **2015**, *17*, 053023.

(41) Zhang, D.; Ha, J.; Baek, H.; Chan, Y.-H.; Natterer, F. D.; Myers, A. F.; Schumacher, J. D.; Cullen, W. G.; Davydov, A. V.; Kuk, Y.; Chou, M. Y.; Zhitenev, N. B.; Strocio, J. A. Strain Engineering a 4a × √3a Charge-density-wave Phase in Transition-metal Dichalcogenide 1T-VSe₂. *Physical review materials* **2017**, *1*, 024005.

(42) Fumega, A. O.; Pardo, V. Absence of Ferromagnetism in VSe₂ Caused by Its Charge Density Wave Phase. **2018**, arXiv:1804.07102. arXiv.org e-Print Archive. <https://arxiv.org/abs/1804.07102> (accessed 21 Apr 2018).

(43) Yu, X.; Hwang, C.; Jozwiak, C.; Köhl, A.; Schmid, A.; Lanzara, A. New Synthesis Method for the Growth of Epitaxial Graphene. *J. Electron Spectrosc. Relat. Phenom.* **2011**, *184*, 100–106.

(44) Barua, S.; Hatnean, M. C.; Lees, M.; Balakrishnan, G. Signatures of the Kondo Effect in VSe₂. *Sci. Rep.* **2017**, *7*, 10964.

(45) Blaha, P.; Schwarz, K.; Madsen, G.; Kvasnicka, D.; Luitz, J. *WIEN2k, an Augmented Plane Wave + Local Orbitals Program for Calculating Crystal Properties*; Technische Universität Wien: Vienna, Austria, 2001.

(46) Perdew, J. P.; Burke, K.; Ernzerhof, M. Generalized Gradient Approximation Made Simple. *Phys. Rev. Lett.* **1996**, *77*, 3865–3868.